HOKKAIDO UNIVERSITY

Title	Efficient operation of atomic frequency comb optical memory using an optical frequency comb in 167Er3+:Y2SiO5
Author(s)	Yasui, Shoichiro; Inaba, Tomohiro; Ishizawa, Atsushi et al.
Citation	Optics Continuum, 3(5), 833-843 https://doi.org/10.1364/optcon.525926
Issue Date	2024-05-15
Doc URL	https://hdl.handle.net/2115/98792
Rights	©2024 Optica Publishing Group under the terms of the Open Access Publishing Agreement. Users may use, reuse, and build upon the article, or use the article for text or data mining, so long as such uses are for non-commercial purposes and appropriate attribution is maintained. All other rights are reserved.
Type	journal article
File Information	Opt. Continuum 3-5_833-843.pdf

Hokkaido University Collection of Scholarly and Academic Papers : HUSCAP

Research Article Vol. 3, No. 5 / 15 May 2024 / Optics Continuum 833
OPTICS CONTINUUM

Efficient operation of atomic frequency comb optical memory using an optical frequency comb in $^{167}Er^{3+}$:Y_2SiO_5

Shoichiro Yasui,[1,2] Tomohiro Inaba,[1] Atsushi Ishizawa,[3] Kenichi Hitachi,[1] Hiroo Omi,[4] Kyuma Matsuura,[2] Reina Kaji,[2] Takehiko Tawara,[5] Satoru Adachi,[2] Xuejun Xu,[1,*] and Haruki Sanada[1]

[1]NTT Basic Research Laboratories, NTT Corporation, Atsugi, Kanagawa 243–0198, Japan
[2]Graduate School of Engineering, Hokkaido University, Sapporo, Hokkaido 060–8628, Japan
[3]College of Industrial Technology, Nihon University, Narashino, Chiba 275–8575, Japan
[4]Faculty of Science and Engineering, Yamato University, Suita, Osaka 564-0082, Japan
[5]College of Engineering, Nihon University, Koriyama, Fukushima 963–8642, Japan
[*]xuejun.xu@ntt.com

Abstract: We demonstrated a highly efficient optical memory operation using an atomic frequency comb (AFC) created from a spectrally flattened optical frequency comb with an isotopically pure $^{167}Er^{3+}$:Y_2SiO_5 crystal under zero magnetic field. Compared with standard AFC creation methods such as pulse train method, our method, called comb transfer method, can create a broadband and high-efficiency AFC at lower power and with less effort. This technique can make a significant improvement in the quality of AFCs in crystals doped with low concentrations of rare-earth ions.

© 2024 Optica Publishing Group under the terms of the Optica Open Access Publishing Agreement

1. Introduction

A quantum memory (QM) capable of storing optical quantum bits is a key to realizing a global quantum information and communication network [1–3]. There, optical qubits suitable for transferring quantum information must be efficiently and reversibly mapped onto spin qubits in solids. For this reason, rare-earth ion-doped crystals, which have been reported to have very long coherence times, have been actively investigated as QM materials [4–6]. Among them, $^{167}Er^{3+}$:Y_2SiO_5 (YSO) has attracted much attention as a crystal with optical transitions interacting with telecommunication wavelength photons suitable for long-distance transfer [7,8]. This crystal has a relatively long population lifetime and optical coherence time due to its robustness against electrical and magnetic perturbations caused by Coulomb shielding by closed-shell electrons outside the 4*f* orbitals and superhyperfine interactions due to the low nuclear spin bath host crystal, YSO [9–11].

As a method to achieve a memory operation while compensating for the small light-matter interactions unique to rare-earth ions, various types of absorption-based optical quantum memory using an ion ensemble have been investigated. Photon-echo based quantum memory protocols, such as revival of silenced echo [12], controlled reversible inhomogeneous broadening/gradient echo memory [13,14], noiseless photon-echo [15], and atomic frequency comb (AFC) [16], have been developed. Among them, the AFC QM protocol has been the most successful in view of multimodality and fidelity. For these QM, the memory time can be improved to a few seconds or more by applying a magnetic field to freeze the nuclear spins [11] and/or by mapping between optical coherence and hyperfine (HF) coherence, known as spin wave storage [17]. The memory efficiency, the power ratio between writing and reading-out pulses, is of course an important property, as is memory time, and the bandwidth, the useful spectral range that the memory

#525926 https://doi.org/10.1364/OPTCON.525926
Journal © 2024 Received 24 Apr 2024; accepted 27 Apr 2024; published 15 May 2024

OPTICS CONTINUUM

can accept, is an equally important property for QM because of the efficient interaction with entangled photon sources and multimodality.

Optical pumping with pulse pairs is a widely used for creating AFC as a standard AFC creation method, but it requires a high optical peak intensity to compensate for the narrow pulse time width to achieve a broadband memory. Furthermore, optical pumping with a continuous fringe-like optical spectrum leads to a decrease in memory efficiency due to a decrease in the optical depth (OD) magnitude and uniformity [18]. Therefore, there is still scope for improvement with respect to memory bandwidth and memory efficiency [19].

In this study, we developed a spectrally flattened optical frequency comb (OFC)-based AFC creation method for $^{167}Er^{3+}$:YSO that enables the creation of high-quality AFCs with high memory efficiency and memory bandwidth. Compared with the standard AFC creation method using the pulse train (PT) method, our method, named the comb transfer (CT) method, can create broadband AFC with superior uniformity and a large optical depth (OD) at lower power in a more straightforward process. It is also superior to the frequency modulation (FM) method [20] in that it produces a flat optical spectrum composed of more uniform comb teeth. Despite the small OD of a sample with a low $^{167}Er^{3+}$ concentration (10 ppm), a memory efficiency of $4.10 \pm 1.02\%$ and a memory bandwidth of 30 MHz were achieved with a memory time of 0.5 µs under zero magnetic field. The frequency sweep of the OFC optimized the comb finesse, which further improved memory efficiency. Furthermore, to confirm that the broadband AFC memory created by the CT method can also store the optical phase information, we performed the interferometric measurements using time-bin qubits and revealed that the relative phase of the time-bin pulses with and without storage is well preserved.

2. Advantages of CT method in the preparation of an AFC

The standard method of AFC production, the PT method, is a very well thought-out one that involves Fourier transforming an arbitrarily shaped optical spectrum into the time domain and using the resulting temporal pulse pairs as the pumping light. As shown in Fig. 1(a), in the simplest time sequence of the PT method, the fringe-shaped optical spectrum generated by the pulse pair is used for optical pumping [21–23]. To achieve high memory efficiency, the key structural parameters of the AFC [OD d, comb finesse F, background depth (BD) d_0] must be optimized [18]. However, since a spectral hole has a finite hole width, as the comb spacing Δ approaches the hole width, i.e., as the memory time increases, the OD decreases because the spectral holes overlap [Fig. 1(c)]. Here, we consider the case of the CT method, which uses an EO comb generated by phase and intensity modulation as the pumping light. As shown in Fig. 1(b), when discrete optical pumping with the spectrally flattened OFC is performed in the CT method, the decrease in OD is suppressed up to a memory time of ~ 0.5 µs [Fig. 1(c)]. Here, the comb finesse F decreases with increasing memory time for the PT method and increases for the CT method, both approaching $F = 2$ asymptotically. At a memory time of ~0.5 µs, the CT method obtains $F = 1.6$ while maintaining the maximum OD unlike in the PT method.

The memory efficiency depends greatly on the shape of the AFC tooth: in the PT method, the shape of the AFC changes from Lorentzian to Gaussian as the memory time increases, whereas in the CT method, the AFC shape changes from rectangular to Gaussian. This is because the comb spacing Δ approaches the hole width Γ_{hole} as the memory time increases, and the AFC naturally changes into one having a Gaussian shape due to the hole overlap. The memory efficiency of an arbitrary AFC shape can be expressed using the key parameters (d, F, d_0) as follows:

$$\eta = (d/F)^2 e^{-d/F} \cdot \left(\frac{\mathcal{F}[n(f)]|_{t=1/\Delta}}{\mathcal{F}[n(f)]|_{t=0}} \right)^2 \cdot e^{-d_0} . \tag{1}$$

The first factor $(d/F)^2 e^{-d/F}$ represents the absorption contribution of the input pulse and re-absorption of the echo signal during propagation through the sample. The second factor

OPTICS CONTINUUM

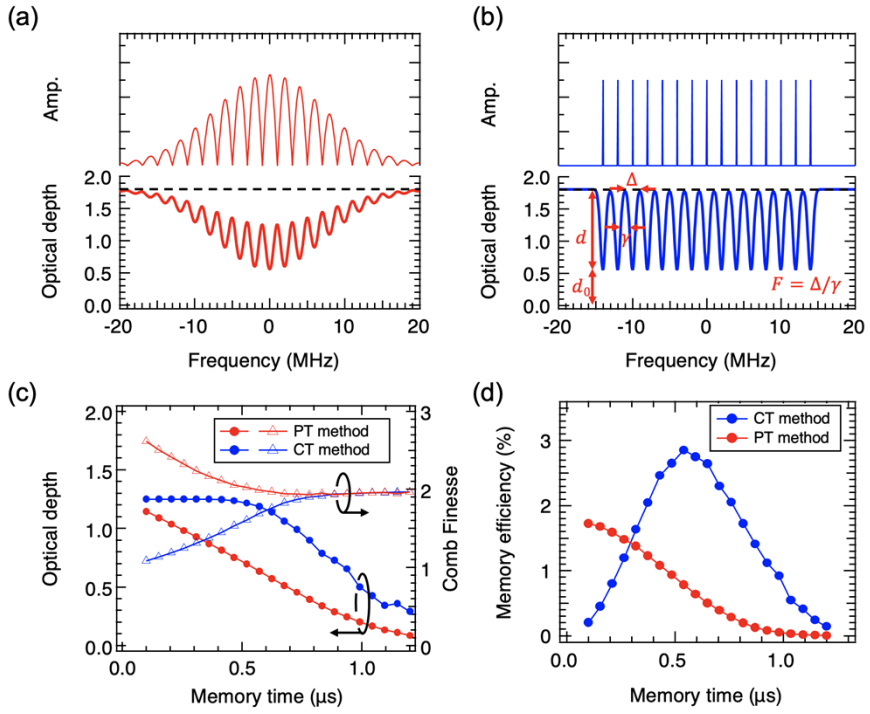

Fig. 1. Simulated optical spectra (top panels) and AFC spectra (bottom panels) by using (a) the PT method and (b) the CT method. Details of the simulation of the AFC spectra are described in Appendix A1. For both methods, the memory bandwidth was set to 20 MHz. The comb spacing was set to $\Delta = 2$ MHz, the OD of the inhomogeneous broadening was set to $d_{\mathrm{inh}} = 1.8$ (horizontal dashed line), the background depth was set to $d_0 = 0.55$, and the hole width (FWHM) was set to $\Gamma_{\mathrm{hole}} = 0.8$ MHz. The key structural parameters of the AFC are shown in red. (c) Simulated memory time dependence ($t_m = 1/\Delta$) of OD (solid circles) and comb finesse F (open triangles) of AFC produced by each method. (d) The expected memory time dependence of the memory efficiency in the PT method (red circles) and CT method (blue circles) for the parameters obtained from the simulations. The efficiency on the left side of the peak efficiency for the CT method can be improved by reshaping the AFC teeth by sweeping the frequency of the OFC, as shown in Fig. 4(c).

represents the loss due to intrinsic dephasing reflecting the AFC shape. The details of the second factor are described in Appendix A1. The third factor e^{-d_0} represents the loss due to background electrons that do not constitute the AFC. Here, the second factor represents the intensity ratio between $t = 1/\Delta$ and $t = 0$ of the Fourier-transformed time-domain waveform of the normalized AFC spectrum $n(f)$. As shown in Fig. 1(d), the memory efficiency of the PT method decreases as the memory time increases, while the CT method has an optimal memory efficiency of 2.94% at $t_m = 0.51$ μs. For a long memory time ($t_m \geq 0.3$ μs), the CT method has a higher memory efficiency than the PT method does. The memory time with maximal memory efficiency is determined in the CT method by the balance between the spectral hole width and comb spacing. Since the hole width at 1% of maximum amplitude is $2.57\Gamma_{\mathrm{hole}} = 2.06$ MHz, if the comb spacing Δ matches this hem width $2.57\Gamma_{\mathrm{hole}}$, the hole overlap in the spectrum is sufficiently suppressed and maximal memory efficiency can be obtained. The peak of memory efficiency can be shifted to a longer memory time by suppressing the homogeneous linewidth that corresponds to the hole width. The memory efficiency in the shorter memory time region of Fig. 1(d) can be improved by sweeping the OFC frequency, as will be shown later in the experiment.

OPTICS CONTINUUM

In addition, the CT method can reduce the peak intensity of the pumping pulse compared with the PT method. Here, let I denote the average light intensity required for optical pumping. The peak intensity of a pulse pair to create an AFC with a memory bandwidth of Γ_{band} is expressed as $I_{\mathrm{Peak}} \sim TI\Gamma_{\mathrm{band}}/2$, where T is the pulse sequence period. In the PT method, to generate a fringe-like optical spectrum, the Fourier limitation, $1/T$, must be sufficiently smaller than the comb width, γ [24]. Therefore, I_{Peak} depends on the memory bandwidth and must be sufficiently large. The CT method, on the other hand, uses a $1/\Delta$-period gating operation to extract only the downchirp from the phase-modulated CW light. Therefore, the required peak intensity is $I_{\mathrm{Peak}} = 2I$. The memory bandwidth is expressed as $\Gamma_{\mathrm{band}} = 2\Delta\Theta$ in terms of the modulation index Θ. In the PT method, it is necessary to reduce the pulse width ($1/\Gamma_{\mathrm{band}}$) and increase I_{Peak} to expand Γ_{band}, whereas, in the CT method, it can be expanded simply by increasing the modulation index Θ regardless of the peak intensity. For example, in this study, we used an OFC with $I = 8$ μW average pump intensity ($I_{\mathrm{Peak}} = 16$ μW) and 30-MHz memory bandwidth Γ_{band}. If the PT method were used to create the AFC with the same Γ_{band}, the required peak intensity would be $I_{\mathrm{Peak}} = 24$ mW for $T = 100$ μs. Furthermore, the CT method can be used in combination with the burn back (BB) method [25–27] and can contribute to broadening the bandwidth of the BB method. Although a pulsed laser was recently proposed as a way to partially address the issue of peak intensity [28], to obtain AFC with a broad memory bandwidth in the PT method, the average intensity of the pulse laser source must be strong, and it is basically difficult to produce more complex pulse waveforms.

As shown above, the CT method can achieve an OD about twice that of the PT method at the optimum memory time t_m without significantly compromising the comb finesse F. In addition, an arbitrary comb finesse can be achieved by performing a frequency sweep of the OFC. Furthermore, the memory bandwidth does not depend on the peak intensity and can be easily increased by improving the phase modulation depth. Recently, there were reports on improvements to the PT method by using numerous adiabatic pulse trains to optimize the AFC tooth shape [24,29,30]. However, these methods typically require creation of complex pulse waveforms, and therefore highly delicate control with advanced instruments, whereas the CT method is simpler and more straightforward.

Compared with the previously reported FM method [20], which generates OFC by internal modulation in the laser cavity, the CT method that generates OFC by using external modulation has several advantages. First, external modulation would not disturb the frequency locking of the laser itself, whereas internal modulation would inevitably disturb the locking, thus requiring a complicated locking scheme, as shown in the previous work [20]. Second, our method provides much more flexibility than the previous one in the sense that additional intensity modulation can be easily added to the pumping laser; thus, more sophisticated and complex modulation formats can be produced straightforwardly. In this study, for example, using EOM in combination with AOM enabled only the down-chirp of the phase modulation to be extracted by using intensity modulation. So, each optical mode has almost the same optical intensity, which is very important to creating AFCs with a uniform width and depth. Finally, the EO comb is a simple method that does not require advanced technology, since it is now commercially available.

3. Sample and measurement system

Figure 2(a) shows the AFC echo measurement system used in this study. An optical frequency stabilized external cavity laser diode (ECLD: RIO, Grande) with a linewidth of 1 kHz was used as a C-band CW laser source. As described in Ref. [9], the optical frequency fluctuations of the ECLD were stabilized below 10 Hz by phase-locking to a 100-MHz repetition rate fiber laser comb. The laser beam was divided into a pumping path (Pump) to produce the AFC, a preparation path (Prep.) to partially initialize the population of $^{167}Er^{3+}$:YSO, and a signal path (Input/Probe) to produce the write pulse to be stored. To observe the AFC spectrum, the first-order optical

OPTICS CONTINUUM

sideband was generated by using intensity-modulation type electro-optic modulators (EOMs: iXblue, MX-LN) and band-pass filters (BPFs: Yenista, XTM-50) on the respective paths. An erbium doped fiber amplifier (EDFA: KEOPSYS, CEFA) was placed on the Prep. and Pump paths to compensate for the light intensity reduction due to the optical elements. Acousto-optic modulators (AOMs: Gooch & Housego, Fibre-Q) were used to obtain the Input pulses with Gaussian waveforms in time-domain. The temporal width (FWHM) of the Input pulse was 50 ns, requiring a memory bandwidth of 20 MHz. The two EOMs were connected in series to increase the phase modulation depth and extend the bandwidth of the OFC. The obtained modulation index was $\Theta \sim 4\pi$, and the bandwidth of the OFC was about 40 MHz when creating an OFC with 2-MHz spacing. In addition, the OFC was flattened by selectively gating the linear part of the downchirp in the phase modulation with an AOM [31]. The average intensity of the Pump beam was 8 μW. The AFC spectrum was monitored using a digital oscilloscope (Tektronix: MSO64), and the AFC echo was observed using a superconducting nanowire single photon detector (SNSPD: Single Quantum, 78% quantum efficiency). To eliminate the strong residual Pump and Prep. photons from measured echo signal, we controlled the timing of an optical switch (O-switch: HAPHIT, FOMS) for the Pump and Prep. pulses and an AOM inserted just before the detector.

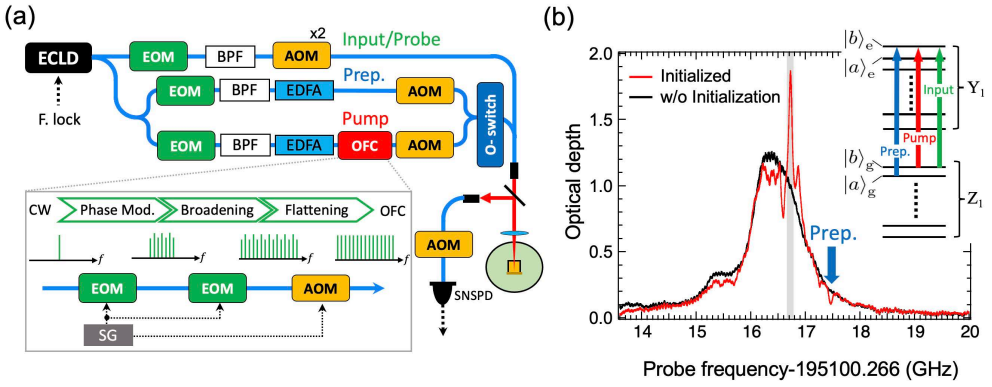

Fig. 2. (a) Schematic diagram of the measurement system. (b) Inhomogeneously broadened spectrum of the $^4I_{15/2}$ (Z_1)-$^4I_{13/2}$ (Y_1) optical transition (black line) and partially initialized spectrum (red line) by optical pumping at the excitation frequency (195117.666 GHz) indicated by the blue arrow. The inset shows the HF sublevels belonging to Z_1 and Y_1 and the optical transition of each beam path. The HF sublevels are described by $|m_s, m_I\rangle_{g(e)}$ using the quantum numbers of electron spin m_s and nuclear spin m_I. The levels $|a\rangle_g$ and $|b\rangle_g$ ($|a\rangle_e$, and $|b\rangle_e$) correspond to the upper two HF sublevels of Z_1 (Y_1), and $|a\rangle_{g(e)}$ ($|b\rangle_{g(e)}$) consists of degenerate HF sublevels of $|+1/2, -3/2\rangle_{g(e)}$ and $|+1/2, -1/2\rangle_{g(e)}$ ($|+1/2, -7/2\rangle_{g(e)}$ and $|+1/2, -5/2\rangle_{g(e)}$).

The sample was an isotopically pure $^{167}Er^{3+}$:YSO crystal ($^{167}Er^{3+}$ concentration is 10 ppm) grown by the Czochralski method [10]. It was cut into a cuboid with a size of 5 × 5 × 6 mm (D_1 × D_2 × b axes) and placed in a cryogen-free cryostat with optical windows, which allow optical access to the sample from outside the cryostat. Measurements were performed at 1.57 K and zero magnetic field. The laser beam was incident along the b-axis and was reflected by a Au mirror placed at the end of the sample. Thus, it passed through the sample twice. The interaction length between the light and $^{167}Er^{3+}$ ions was 12 mm, and the OD of the inhomogeneous broadening of the site 1 $^4I_{15/2}$ (Z_1)-$^4I_{13/2}$ (Y_1) optical transition was $d_{inh} \sim 1.2$. Pulses with a temporal width (FWHM) of 15 ns, repetition period of 4.2 μs, and average intensity of 34 μW were sent on the Prep. path. The pulses swept out the population over a width of 66 MHz in $|a\rangle_g$ to the other HF sublevels and increased the population of $|b\rangle_g$ levels detuned by 740 MHz. As shown in Fig. 2(b),

OPTICS CONTINUUM

the OD of the inhomogeneous broadening was d_{inh} ~1.8 when such a partial state initialization was performed using the light on the Prep. path.

4. Results and discussion

Figure 3(a) shows the optical spectrum of a spectrally flattened OFC with a 2-MHz comb spacing and the AFC spectrum produced by the CT method. The OFC spectrum has a flat intensity in a range wider than 20 MHz, and the OD of each tooth in the transferred and created AFC is uniform. The results of a fitting by a super Gaussian function show that the OD d is 1.18, comb finesse F is 1.62, and BD d_0 is 0.53. The hole width was 0.83 MHz from a fitting by a Gaussian function. As shown in Ref. [18] and Fig. 1(a), the overlap of the hole spectra causes a loss in OD when an AFC with $\Delta = 2$ MHz is created by the PT method, but such a decrease is not observed in the CT method. The key to increasing the time multiplicity of the AFC QM is to increase the memory bandwidth [32]. In the CT method, if more EOMs are placed in series as shown in Ref. [31,33] to generate the OFC, it is possible to set the modulation index to $\Theta \sim 20\pi$. In this case, the memory bandwidth is about 250 MHz at a comb spacing Δ of 2 MHz, which is comparable to the inhomogeneous broadening of $^{167}Er^{3+}$:YSO.

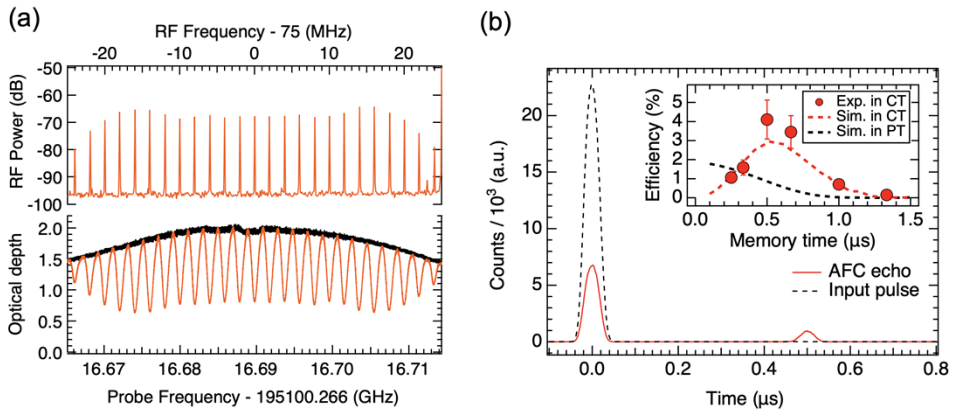

Fig. 3. (a) Created spectrally flattened OFC spectrum [top panel] and AFC spectrum [bottom panel]. The black curve indicates partially initialized inhomogeneous broadening. (b) AFC echo measurement results. The solid red line shows the transmitted pulse and echo signal, and the dotted black line shows the input pulse. The red plot in the inset shows the memory efficiency as a function of memory time. Error bars represent the standard deviation of five measurements. The dotted red and black lines represent simulated results using the CT and PT methods shown in Fig. 2(d).

The AFC echo signal read out from the AFC created by the CT method is shown in Fig. 3(b). The echo signal clearly appeared at $t = 0.5$ μs, which corresponds to the inverse of the comb spacing $\Delta = 2$ MHz. The highest efficiency of $4.10 \pm 1.02\%$ was obtained when the memory time was 0.5 μs. The inset shows the memory time dependence of the memory efficiency obtained when the comb spacing of the OFC was varied. The estimated memory efficiency [Fig. 1(d)] obtained from the AFC spectra was in approximate agreement with the measured results. The deviations possibly arise from fluctuations in the light intensity of the input pulses. For shorter memory times, the decoherence contribution from the inhomogeneous broadening within a single tooth increases as the comb finesse decreases, resulting in a decrease in memory efficiency. On the other hand, for longer memory times, the sudden decrease in OD due to the overlap of the hole spectra leads to a decrease in memory efficiency.

OPTICS CONTINUUM

Next, the comb finesse of the AFC was controlled by fixing the comb spacing of the OFC at 4 MHz and sweeping the frequency of the OFC itself with a period of 1 ms. Figure 4(a) shows that the finesse of the AFC was well controlled by varying the sweep frequency. The dependence of the key parameters (F, d, d_0) on the sweep frequency is shown in Fig. 4(b). A decrease in d and an increase in d_0 occurred as the sweep frequency was increased. This can be attributed to a decrease in the pumping intensity per unit frequency. When the sweep frequency exceeds 3 MHz, the hole spectra will begin to overlap and the OD decreases rapidly.

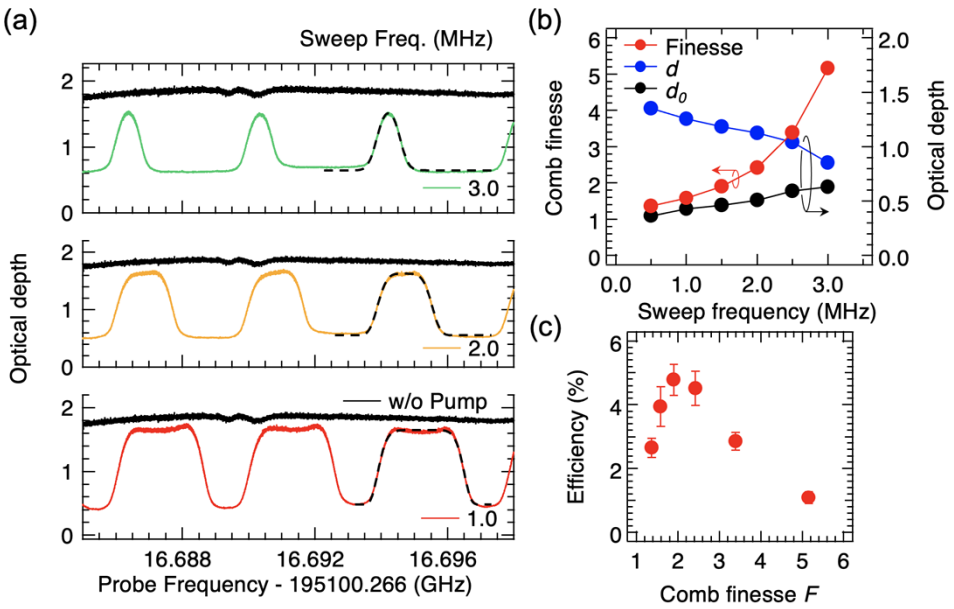

Fig. 4. (a) AFC spectrum when the OFC is frequency swept; swept frequencies of 1 MHz (bottom panel), 2 MHz (middle panel), and 3 MHz (top panel) are shown. The solid black lines represent partially initialized inhomogeneous broadening. The black dotted lines represent the fitting curves with a super Gaussian function. (b) Sweep frequency dependence of comb finesse (red), OD (blue), and BD (black). (c) Comb finesse dependence of memory efficiency obtained from echo measurements (red circles). Error bars represent the standard deviation of five measurements.

Finally, echo measurements were performed to estimate the memory efficiency under the different comb finesse conditions. Figure 4(c) shows the comb finesse dependence of the memory efficiency. The memory efficiency was improved by changing the OFC sweep frequency and optimizing the comb finesse, and a maximum efficiency of $4.77 \pm 0.48\%$ was obtained at a sweep frequency of 1.5 MHz and memory time of 0.25 µs. This improvement in efficiency was achieved at Δ=4 MHz (t_m = 0.25 µs), but the same level of improvement can be obtained at other t_m (< 0.5 µs) as well.

To confirm that the present AFC memory can also store the optical phase information, we performed echo measurements using time-bin pulses, which are used as qubits (time-bin qubits) in quantum internet research [19]. When writing and reading-out a time-bin qubit using the AFC, the optical phase information after readout must be preserved. To confirm the preservation of the phase information, the relative phase change and visibility of the readout time-bin pulses to the written time-bin pulses were investigated by making interferometric measurements. The write optical pulse was input to an asymmetric Mach-Zehnder interferometer (uMZI$_1$) with an optical path difference of 15 m, and then time-bin optical pulses with a time interval of 75 ns were produced. The relative phase $\Delta\phi_1$ of the time-bin pulses was stabilized through feedback

OPTICS CONTINUUM

control using a fiber stretcher (Optiphase, PZ3-PM2). The write or read-out pulses were then input to $uMZI_2$ to perform a projection measurement of the interference phase. The coherence was evaluated by sweeping the relative phase $\Delta\phi_2$ of $uMZI_2$ by averaging the number of detected counts over a time bandwidth of 100 ns at the superposition of two-time bins detected by SNSPD.

As shown in Fig. 5(a), Interference originating from the relative phase between the two pulses of the time bin was clearly observed both with and without a memory component. The respective sinusoidal interference signals were fitted using $f(\Delta\phi_2) = A[1 + \cos\{\Delta\phi_2 - \phi_{w(w/o)}\}]$. Here, $\phi_{w(w/o)}$ is the sum of the interference phase offset derived from the measurement system and the relative phase $\Delta\phi_1$ of the time-bin pulses. The difference $\phi_w - \phi_{w/o}$ represents the change in the relative phase $\Delta\phi_1$ with and without the memory component. The obtained change in the interference phase was $\phi_w - \phi_{w/o} = 0.05\pi \pm 0.022\pi$. This small difference is considered to be due to fluctuations in the relative phase and polarization caused by interferometer instability. If we define visibility as $V = (V_{max} - V_{min})/(V_{max} + V_{min})$ and use the counts at $\Delta\phi_2 = 0.7\pi$ and $\Delta\phi_2 = 1.7\pi$ as V_{max} and V_{min}, respectively, the visibility of the write pulses is $96.4 \pm 0.11\%$ and that of the readout pulses is $93.3 \pm 1.06\%$. The average photon number per the readout pulse was 5.2, suggesting that the background light reduced the visibility. When the average photon count of background light (6.33) was subtracted, the visibility with memory component was $100.54 \pm 1.23\%$.

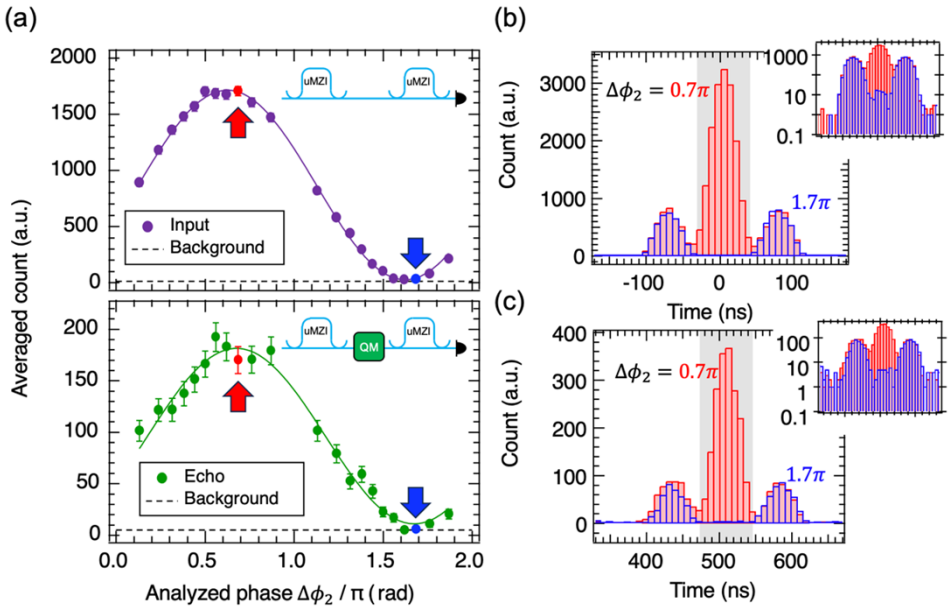

Fig. 5. (a) Time-bin pulses coherence measurements without (top panel) and with (bottom panel) memory. The inset shows a schematic diagram of the measurement system. The horizontal axis represents the relative phase $\Delta\phi_2$ of the asymmetric Mach-Zehnder interferometer (uMZI) on the detector side. The red and blue circles show the counts at $\Delta\phi_2 = 0.7\pi$ and $\Delta\phi_2 = 1.7\pi$, respectively. Time histograms of the interference signal without (b) and with (c) memory. Histograms with red and blue bars correspond to the distribution at the red and blue points in Fig. 5(a). The inset shows the case where the vertical axis is a logarithmic scale.

On the basis of these results, we can conclude that an AFC with uniform OD over a bandwidth of 30 MHz was created by mapping the spectrally flattened OFC to the AFC, and a memory efficiency of $4.1 \pm 1.02\%$ was achieved with a memory time of 0.5 µs. Further, when the frequency sweep of the OFC was used, the comb finesse F could be controlled and a memory efficiency of

OPTICS CONTINUUM

$4.77 \pm 0.48\%$ achieved at a memory time of 0.25 μs. The upper limit of memory efficiency is bottlenecked by d_{inh} and the absorption d_0, but it can be improved by increasing the interaction length [34] and by using cavity QED [35–37]. In addition, the relative phase change and visibility of the echo signal readout of the CT method do not show significant degradation, suggesting that the degradation in fidelity is small even when the time-bin qubit is stored.

Because the experiments presented here were performed under zero magnetic field, the lifetime of HF sublevels T_1^{hyp} was expected to be as short as ~350 ms [18], making a full state initialization difficult. A promising way of extending T_1^{hyp} would be applying a magnetic field, which suppresses spin-flip-flop and spin-lattice relaxation [25], and the resultant full state initialization could be expected to further improve memory efficiency.

Moreover, to further extend the memory time, it is necessary to implement the full memory protocol based on spin wave storage by using zero first order Zeeman (ZEFOZ) transitions. As predicted by S.-J. Wang et al., by utilizing ZEFOZ transitions and setting the optimum applied field strength and angle, the coherence time of HF sublevels T_1^{hyp} could be longer than 1 s for $^{167}Er^{3+}$:YSO with similar Er concentration used in this study [38]. J. Stuart et al. has also suggested the possibility of spin wave storage in $^{167}Er^{3+}$:YSO [25]. In order to experimentally realize spin wave storage, however, several technical issues have to be addressed, for example, determination of ZEFOZ transitions with long coherence times from the complicated HF structure, mitigation of dephasing caused by the inhomogeneous spin linewidth of HF transitions, and so on. All of these issues will be subjected of further investigation.

5. Conclusion

We demonstrated an AFC-based optical memory using a simple CT method in $^{167}Er^{3+}$:YSO under zero magnetic field and showed that it can achieve relatively high memory efficiency with less OD loss than in the PT method. Compared with the PT method, it could more easily create an AFC with the same memory bandwidth by using spectrally flattened OFC with a smaller optical peak intensity. The memory efficiency was optimized to $4.77 \pm 0.48\%$ by controlling the comb finesse. This method can easily improve the optical depth and comb finesse, which determine the efficiency of AFC, and is applicable to many rare-earth ion crystals.

Appendix

A1. Simulation of AFC spectra and memory efficiency

This appendix details the simulation of the AFC spectrum performed in this study.

To reproduce the AFC shape, we consider the normalized OFC optical spectrum $h(f)$ and the normalized hole spectrum $g(f,f_0) = \exp[-4\ln 2\{(f-f_0)/\Gamma_{\mathrm{hole}}\}^2]$ generated when CW light is radiated over an inhomogeneous broadening. Here, Γ_{hole} means the actual hole FWHM considering power broadening. The AFC shape $n(f)$ is reproduced by convolving and normalizing $h(f)$ and $g(f,f_0)$ with respect to f_0 according to the following equation.

$$n(f) = -\int_{-\infty}^{\infty} h(f)g(f,f_0)df_0 \Big/ \int_{-\infty}^{\infty} h(f)g(f,f_0)df_0 \tag{2}$$

The negative sign here reflects that $n(f)$ is an absorption spectrum. The actual AFC spectral shape $d(f)$ can be expressed by scaling with the inhomogeneous broadening OD (d_{inh}) and BD (d_0) as follows.

$$d(f) = (d_{\mathrm{inh}} - d_0)n(f) + d_0 \tag{3}$$

Next, let us examine the memory efficiency of arbitrary AFC shapes. The memory efficiency of the AFC is obtained analytically from the Maxwell-Bloch equation, as described in Ref. [32].

OPTICS CONTINUUM

In particular, the second factor of Eq. (1) is related to intrinsic dephasing in memory due to the comb shape. For example, when the AFC tooth is Gaussian (or rectangular), the factor is $\exp\{-\pi^2/(2F^2\ln 2)\}$ (or $\mathrm{sinc}^2(\pi/F)$), which is consistent with the analytical solution for the memory efficiency of each comb shape reported in Refs. [24 and 32].

Funding. Japan Society for the Promotion of Science (JP21H01745, JP22H01995, JP23H01887, JP23K17883, JP23KJ0051).

Acknowledgments. We thank Dr. Ryuichi Ohta, Dr. Yoji Kunihashi, Prof. Hideki Gotoh, and Prof. Junsaku Nitta for the fruitful discussions.

Disclosures. The authors declare no conflicts of interest.

Data availability. Data underlying the results presented in this paper are not publicly available at this time but may be obtained from the authors upon reasonable request.

References

1. L.-M. Duan, M. D. Lukin, J. I. Cirac, *et al.*, "Long-distance quantum communication with atomic ensembles and linear optics," Nature **414**(6862), 413–418 (2001).
2. H. J. Kimble, "The quantum internet," Nature **453**(7198), 1023–1030 (2008).
3. M. Pompili, S. L. N. Hermans, S. Baier, *et al.*, "Realization of a multinode quantum network of remote solid-state qubits," Science **372**(6539), 259–264 (2021).
4. C. W. Thiel, T. Bttger, and R. L. Cone, "Rare-earth-doped materials for applications in quantum information storage and signal processing," J. Lumin. **131**(3), 353–361 (2011).
5. J. V. Rakonjac, D. Lago-Rivera, A. Seri, *et al.*, "Entanglement between a telecom photon and an on-demand multimode solid-state quantum memory," Phys. Rev. Lett. **127**(21), 210502 (2021).
6. Y. Ma, Y.-Z. Ma, Z.-Q. Zhou, *et al.*, "One-hour coherent optical storage in an atomic frequency comb memory," Nat. Commun. **12**(1), 2381 (2021).
7. O. Guillot-Noël, P. Goldner, Y. Le Du, *et al.*, "Hyperfine interaction of Er^{3+} ions in Y_2SiO_5: An electron paramagnetic resonance spectroscopy study," Phys. Rev. B **74**(21), 214409 (2006).
8. D. Hashimoto and K. Shimizu, "Coherent Raman beat analysis of the hyperfine sublevel coherence properties of $^{167}Er^{3+}$ ions doped in an Y2SiO5 crystal," J. Lumin. **171**, 183–190 (2016).
9. S. Yasui, M. Hiraishi, A. Ishizawa, *et al.*, "Precise spectroscopy of ^{167}Er:Y_2SiO_5 based on laser frequency stabilization using a fiber laser comb," Opt. Express **29**(17), 27137–27148 (2021).
10. T. Tawara, G. Mariani, K. Shimizu, *et al.*, "Effect of isotopic purification on spectral-hole narrowing in $^{167}Er^{3+}$ hyperfine transitions," Appl. Phys. Express **10**(4), 042801 (2017).
11. M. Rančić, M. P. Hedges, R. L. Ahlefeldt, *et al.*, "Coherence time of over a second in a telecom-compatible quantum memory storage material," Nat. Phys. **14**(1), 50–54 (2018).
12. J. Dajczgewand, J.-L. Le Gouët, A. Louchet-Chauvet, *et al.*, "Large efficiency at telecom wavelength for optical quantum memories," Opt. Lett. **39**(9), 2711–2714 (2014).
13. M. P. Hedges, J. J. Longdell, Y. Li, *et al.*, "Efficient quantum memory for light," Nature **465**(7301), 1052–1056 (2010).
14. B. Lauritzen, J. Minář, H. de Riedmatten, *et al.*, "Telecommunication- wavelength solid-state memory at the single photon level," Phys. Rev. Lett. **104**(8), 080502 (2010).
15. Y.-Z. Ma, M. Jin, D.-L. Chen, *et al.*, "Elimination of noise in optically rephased photon echoes," Nat. Commun. **12**(1), 4378 (2021).
16. H. de Riedmatten, M. Afzelius, M. U. Staudt, *et al.*, "A solid-state light-matter interface at the single-photon level," Nature **456**(7223), 773–777 (2008).
17. M. Afzelius, I. Usmani, A. Amari, *et al.*, "Demonstration of atomic frequency comb memory for light with spin-wave storage," Phys. Rev. Lett. **104**(4), 040503 (2010).
18. S. Yasui, M. Hiraishi, A. Ishizawa, *et al.*, "Creation of a high-resolution atomic frequency comb and optimization of the pulse sequence for high-efficiency quantum memory in ^{167}Er:Y_2SiO_5," Opt. Continuum **1**(9), 1896–1908 (2022).
19. Z. -Q. Zhou, C. Liu, C. -F. Li, *et al.*, "Photonic Integrated Quantum Memory in Rare-Earth Doped Solids," Laser Photonics Rev. **17**(10), 2300257 (2023).
20. M. Bonarota, J.-L. Le Gouët, and T. Chanelière, "Highly multimode storage in a crystal," New J. Phys. **13**(1), 013013 (2011).
21. I. Craiciu, M. Lei, J. Rochman, *et al.*, "Nanophotonic quantum storage at telecommunication wavelength," Phys. Rev. Appl. **12**(2), 024062 (2019).
22. T. Chanelière, J. Ruggiero, M. Bonarota, *et al.*, "Efficient light storage in a crystal using an atomic frequency comb," New J. Phys. **12**(2), 023025 (2010).
23. S. Dutta, Y. Zhao, U. Saha, *et al.*, "An atomic frequency comb memory in rare-earth-doped thin-film lithium niobate," ACS Photonics **10**(4), 1104–1109 (2023).
24. P. Jobez, N. Timoney, C. Laplane, *et al.*, "Towards highly multimode optical quantum memory for quantum repeaters," Phys. Rev. Appl. **93**(3), 032327 (2016).

OPTICS CONTINUUM

25. J. Stuart, M. Hedges, R. Ahlefeldt, *et al.*, "Initialization protocol for efficient quantum memories using resolved hyperfine structure," Phys. Rev. Res. **3**(3), L032054 (2021).
26. A. Amari, A. Walther, M. Sabooni, *et al.*, "Towards an efficient atomic frequency comb quantum memory," J. Lumin. **130**(9), 1579–1585 (2010).
27. N. Sinclair, E. Saglamyurek, H. Mallahzadeh, *et al.*, "Spectral multiplexing for scalable quantum photonics using an atomic frequency comb quantum memory and feed-forward control," Phys. Rev. Lett. **113**(5), 053603 (2014).
28. M. Nicolle, J. N. Becker, C. Weinzetl, *et al.*, "Gigahertz-bandwidth optical memory in Pr^{3+}:Y_2SiO_5," Opt. Lett. **46**(12), 2948–2951 (2021).
29. L. Rippe, M. Nilsson, S. Kroll, *et al.*, "Experimental demonstration of efficient and selective population transfer and qubit distillation in a rare-earth-metal-ion-doped crystal," Phys. Rev. A **71**(6), 062328 (2005).
30. M. Bonarota, J. Ruggiero, J. Le Gouët, *et al.*, "Efficiency optimization for atomic frequency comb storage," Phys. Rev. A **81**(3), 033803 (2010).
31. A. Ishizawa, T. Nishikawa, A. Mizutori, *et al.*, "Generation of 120-fs laser pulses at 1-GHz repetition rate derived from continuous wave laser diode," Opt. Express **19**(23), 22402–22409 (2011).
32. M. Afzelius, C. Simon, H. de Riedmatten, *et al.*, "Multimode quantum memory based on atomic frequency combs," Phys. Rev. A **79**(5), 052329 (2009).
33. A. Ishizawa, T. Nishikawa, K. Hitachi, *et al.*, "Optical-referenceless optical frequency counter with twelve-digit absolute accuracy," Sci. Rep. **13**(1), 8750 (2023).
34. A. Ortu, A. Tiranov, S. Welinski, *et al.*, "Simultaneous coherence enhancement of optical and microwave transitions in solid-state electronic spins," Nat. Mater. **17**(8), 671–675 (2018).
35. M Afzelius and C. Simon, "Impedance-matched cavity quantum memory," Phys. Rev. A **82**(2), 022310 (2010).
36. M. Sabooni, Q. Li, S. Kröll, *et al.*, "Efficient quantum memory using a weakly absorbing sample," Phys. Rev. Lett. **110**(13), 133604 (2013).
37. P. Jobez, I. Usmani, N. Timoney, *et al.*, "Cavity-enhanced storage in an optical spin-wave memory," New J. Phys. **16**(8), 083005 (2014).
38. S.-J. Wang, Y.-H. Chen, J. J. longdell, *et al.*, "Hyperfine states of erbium doped yttrium orthosilicate for long-coherence-time quantum memories," J. Lumin. **262**, 119935 (2023).